1D Simulation of Avalanche to Streamer to Spark Transition of Plasma Discharge in Ammonia-Air Combustion

Taaresh Sanjeev Taneja* and Suo Yang[†]

Department of Mechanical Engineering, University of Minnesota – Twin Cities, Minneapolis, MN 55455, USA

Hariswaran Sitaraman[‡]

Computational Science Center, National Renewable Energy Laboratory, Golden, CO 15013, USA

The backward problem of plasma assisted combustion emphasizes evaluating the effect of the evolving thermochemical state on the plasma discharge. This paper investigates the dependence of avalanche to streamer to spark formation dynamics and kinetics on the gas composition and temperature at different points in an ammonia-air premixed laminar flame using a self-consistent multigrid-based 1D plasma solver. Different values of α , the coefficient for effective ionization events per unit length, have been reported for electron avalanches in air and stoichiometric NH3-air mixtures. The streamer inception has been shown to obey the Meek's criterion. An exponential reduction in streamer and spark formation time has been observed from plasma simulations at different points in the unburnt, pre-heat zone, reaction zone and the fully burnt regions of the premixed flame. While the enhancement of the reduced electric field with increasing temperature affects effective ionization, there exists a minimum breakdown field for streamer formation, which does not vary proportionally with the changing number density of the gas. The change in the mixture from reactants (NH_3, O_2, N_2) to products of complete combustion of ammonia in air (N₂, H₂O) has also been shown to affect the streamer and spark formation. Finally, the major pathways during the streamer and spark phases which are responsible for producing important radicals used in combustion of NH₃ are also discussed.

I. Nomenclature

```
Ionization events per unit length (mm^{-1})
\alpha
           Gas pressure, (Pa, torr, atm)
p
d
           Distance from the cathode (mm)
           Number density of species k (m^{-3})
n_k
           Time (s)
           Density Flux of species k (m^{-2}s^{-1})
\Gamma_k
           Production (Gain) rate of species k (m^{-3}s^{-1})
\dot{G}_k
           Consumption (Loss) rate of species k (m^{-3}s^{-1})
\dot{L}_k
           Mobility of species k (m^2V^{-1}s^{-1})
\mu_k
           Diffusion coefficient of species k in the background gas mixture (m^2s^{-1})
D_k
\vec{E}
           Electric field (V/m)
φ
           Electric potential (V)
           Permittivity of free space (Fcm^{-1})
\epsilon_0
           Charge of a single electron, -1.602 \times 10^{-19} C
Z_k
           Charge of species k
           Electron energy density (Jm^{-3})
           Flux of electron energy density (Jm^{-2}s^{-1})
           Net source term of electron energy density (Jm^{-3}s^{-1})
           Electron temperature (K / eV)
```

^{*}Ph.D. Candidate, Student Member AIAA.

[†]Richard & Barbara Nelson Assistant Professor, suo-yang@umn.edu (Corresponding Author), Senior Member AIAA.

[‡]Researcher IV - Mechanical Engineering, Member AIAA.

 T_g = Gas and ion temperature (K) n_e = Electron number density (m^{-3})

 k_B = Boltzmann constant J/K

 m_e = Mass of a single electron, $9.11 \times 10^{-31} kg$

 m_b = Mass of a single molecule of background gas (kg)

 ν = Electron - neutral collision frequency (s^{-1})

II. Introduction

TREAMER formation is a common phenomena in most high-pressure plasmas. The theory of streamer inception and propagation has been explained in depth in Raizer's textbook [1] on gas discharge physics. The deficiencies of Townsend's electron avalanche theory [2] in predicting the formation of streamers observed at high pressures and larger inter-electrode gaps were addressed in Loeb's [3] and Meek's [4] theories, leading to the acceptance of Meek's criterion, which demands that the electric field established by the space charge reaches a value at the order of the external applied electric field and that the breakdown occurs when $\alpha d \approx 18 - 22$. For $pd \gtrsim 200$ Torr-cm, and at sufficiently high applied voltages, electron avalanches starting from the cathode lead to the formation of ions in the gap between the two electrodes. The electrons travel faster towards the anode owing to their polarity and higher mobility, thereby developing a space charge, which creates its own field. If the space charge field is of the same order as the applied field, it amplifies the ionization at a distance proportional to α^{-1} from the negative tail of the space charge layer, which starts the propagation of an ionization wave towards the cathode. Secondary avalanches caused by photo-ionization due to the release of high energy photons during de-excitation of electronic excited states produced in the primary discharge often lead to the creation of secondary electrons, which in turn get attracted by the positive ions produced by the primary avalanche. This keeps enhancing the electric field at the head of the ionization wave, which further leads to increased ionization. Depending on the inter-electrode gap size, applied potential, extent of photionization and the thermochemical state; if the ionization wave reaches the cathode, the streamers form a spark channel, which draws large current from the anode to the cathode, with only a relatively small voltage drop at the cathode [5]. This results in increased production of radicals and heating of the gas, which can be leveraged for ignition of combustible mixtures. 3D particle simulations of streamers for CH₄-air combustion have been performed in Bouwman et al. [6], where they showed the effect of methane addition which leads to streamer branching due to the suppression of photo-ionization. Nijdam et al. [7] contains a very comprehensive review of streamer formation and propagation, where the effects of electron energy losses, photo-ionization, and attachment rates have been discussed to be the major reasons for the difference in streamer dynamics in different gap sizes and thermo-chemical conditions. The difference in the photo-ionization coefficient of a stoichiometric methane-air mixture as compared to pure air has been shown to be the primary reason for the higher electron number density and electric fields at the streamer head in Naidis [8].

This paper specifically focuses on the impact of avalanche to streamer to spark transition for ammonia-air combustion. Given the challenges of ammonia combustion (e.g., high heat of ignition, narrow range of flammability, high NO_x production, etc.), both experimental and computational research has focused on enhancing its ignition and flame stabilization using non-equilibrium plasma [9–17]. The current work aims at computationally investigating the physical and chemical effects associated with avalanche to streamer to spark transition in ammonia-air mixtures to highlight the important radical production mechanisms and time scales of streamer and spark formation in a 1D domain. Moreover, the effects of the thermo-chemical state on the plasma dynamics and kinetics have been evaluated by considering different initial conditions obtained from a 1D laminar premixed flame solution. This has been motivated by the "backward problem" describing the effect of the gas chemistry (combustion) on the plasma discharge in [18].

III. Numerical Methodology

A self-consistent one-dimensional (1D) plasma model with a two-temperature approximation is developed in this work. The model consists of governing evolution equations for electrons, ions, and neutral species density with the drift-diffusion approximation for charged species fluxes, a constitutive Poisson equation to obtain self-consistent electrostatic potential and electric field, and an electron energy equation for computing mean electron temperature which is coupled with electron-impact finite-rate chemistry. A similar 1D solver has been used in other studies exploring streamer dynamics at high pressures [5, 19] and other works on studying dielectric barrier discharges, ignition and reforming at lower pressures in [20–24]. The equations solved are described below.

The evolution of the number density n_k of each species k among N_{sp} species is solved for, using separate conservation

equations where \dot{G}_k and \dot{L}_k are the species production and consumption terms, respectively.

$$\frac{\partial n_k}{\partial t} + \vec{\nabla} \cdot \vec{\Gamma}_k = \dot{G}_k - \dot{L}_k. \tag{1}$$

In Eq. (1), the net flux is estimated using the drift-diffusion approximation:

$$\vec{\Gamma}_k = n_k u_k = \mu_k n_k \vec{E} - D_k \vec{\nabla}(n_k). \tag{2}$$

The mobility for all neutral species is zero, and thus the neutral species transport is only due to diffusion.

The evolution of the electric field, \vec{E} , is governed by the Poisson equation of electric potential ϕ :

$$\nabla^2 \phi + \frac{e}{\epsilon_0} \sum_{k=1}^{N_{sp}} Z_k n_k = 0, \tag{3}$$

$$\vec{E} = -\vec{\nabla}\phi. \tag{4}$$

Finally, the local mean electron energy density, $E_e = 3/2n_e k_B T_e$, is computed by solving Eq. (5):

$$\frac{\partial E_e}{\partial t} + \vec{\nabla} \cdot \vec{\Gamma}_{E_e} = \dot{S}_{E_e},\tag{5}$$

where the flux of electron energy density, $\vec{\Gamma}_{E_e}$, is also calculated using the drift-diffusion model for electron energy $(\epsilon = E_e/n_e)$:

$$\vec{\Gamma}_{E_e} = \mu_{\epsilon} E_e \vec{E} - D_{\epsilon} \vec{\nabla}(E_e), \tag{6}$$

and its source term, \dot{S}_{E_e} , is given by

$$\dot{S}_{E_e} = -e\vec{\Gamma}_e \cdot \vec{E} - \frac{3}{2} n_e k_B (T_e - T_g) \frac{2m_e}{m_b} \nu - \sum_i \Delta E_i r_i. \tag{7}$$

On the right-hand-side (RHS) of Eq. (7), the first term represents the electron Joule heating, the second term is the electron energy loss due to elastic collisions with the gas molecules, and the third term represents the net electron energy loss due to inelastic collisions resulting in excitation, attachment, and ionization of the gas. ΔE_i is the energy associated with the i^{th} electron-impact reaction and r_i is the rate of progress of that reaction.

All the reaction rate coefficients used in calculating the source terms, \dot{G}_k , \dot{L}_k , and \dot{S}_{E_e} , and the electron and electron mean energy transport coefficients (μ_e , D_e , μ_ϵ , D_ϵ) are expressed as functions of the mean electron temperature T_e , which is obtained from the mean electron energy density E_e using $T_e = 2E_e/(3n_ek_B)$, following the local-mean-energy approximation (LMEA). Dirichlet boundary conditions have been applied for the electric potential ϕ at both the electrodes, with one of the electrodes always being held at zero potential (i.e., connected to the ground) and the other being subject to a general time-varying potential (i.e., connected to a power supply). Ion-mobility dominated flux boundary conditions have been applied at the two electrodes for ion number density, depending on the directions of the fluxes of ions, assuming ion quenching at the surface. Maxwellian number density and energy flux are applied for electrons, neutrals, and the electron energy density, using the respective thermal velocities. The gas temperature and pressure are held constant during the nanosecond pulse time-scales used in this work.

Cross section data (from [25]) as a function of electron mean energy is used to obtain the electron-impact reaction rate coefficients and electron transport coefficients, by solving the Boltzmann equation, for which BOLSIG+ [26] has been used. The plasma kinetic mechanism pre-processor, ZDPlasKin [27], is used to generate functions for calculating the reaction rates and the species production / consumption source terms, which are then coupled with the 1D plasma solver.

A Multi-grid 1D Plasma Solver (called "MPS1D") has been developed and used for this work. This code was adapted from the multigrid 3D solver ("MPS3D") described in Sitaraman and Grout [19]. The above listed equations are discretized using the finite volume formulation and are solved on a uniform grid. They are solved in a segregated manner with an implicit Euler time integration scheme. The convective terms are discretized using an upwind discretization for stabilizing high Peclet number electron density and electron energy equations. The diffusive flux is obtained using a second order central scheme. The linear solves during implicit integration is performed using Generalized Minimum Residual (GMRES) method with the geometric multi-grid method [28] as the preconditioner. The Gauss-Seidel method is used as the smoother on successive multi-grid levels.

Table 1 List of reactions used for the He capacitively coupled plasma (CCP) discharge obtained from Yuan and Raja [30].

| No. | Reaction | A | В | С | Energy (eV) |
|-----|---|-------------------------|------|----------|-------------|
| R1 | $E + He \longrightarrow He^* + E$ | 2.308×10^{-10} | 0.31 | 229700.0 | 19.8 |
| R2 | $E + He^* \longrightarrow He + E$ | 1.099×10^{-11} | 0.31 | 0.0 | -19.8 |
| R3 | $E + He \longrightarrow He^+ + 2E$ | 2.584×10^{-12} | 0.68 | 285409.2 | 24.6 |
| R4 | $E + He^* \longrightarrow He^+ + 2E$ | 4.661×10^{-10} | 0.6 | -55460.0 | 4.78 |
| R5 | $E + He_2^* \longrightarrow He_2^+ + 2E$ | 1.268×10^{-12} | 0.71 | 39450.0 | 3.4 |
| R6 | $E + He_2^+ \longrightarrow He^* + He$ | 5.386×10^{-7} | -0.5 | 0.0 | 0.0 |
| R7 | $He^* + He^* \longrightarrow He^+ + He + E$ | 2.7×10^{-10} | 0.0 | 0.0 | -15.0 |
| R8 | $He^* + 2 He \longrightarrow He_2^* + He$ | 1.3×10^{-33} | 0.0 | 0.0 | 0.0 |
| R9 | $He^+ + 2 He \longrightarrow He_2^+ + He$ | 1.0×10^{-31} | 0.0 | 0.0 | 0.0 |

IV. Results and Analysis

A. Solver Verification - Low Pressure CCP Discharge

A capacitively coupled plasma (CCP) discharge in Helium was simulated using MPS1D and the ion density profile was compared against high-fidelity particle-in-cell (PIC) simulation data from Turner et al. [29]. A radio-frequency (RF) plasma source with an AC sinusoidal voltage with a peak of 120 V and a frequency of 13.56 MHz was used to generate a plasma in pure He at a pressure of 1 Torr and room temperature (300 K), resulting in a background gas number density of $3.21 \times 10^{22} m^{-3}$. The gap distance between the two electrodes was set as 6.7 cm, which was discretized using uniformly spaced 513 grid points, and the time step was fixed at 2.3×10^{-11} s. The simulation was initialized with a pre-ionized plasma density of $3.84 \times 10^{14} \text{m}^{-3}$ and was run for a total physical time of $\sim 1.13 \times 10^{-3}$ s. These conditions were replicated exactly from Turner et al.'s paper on bench-marking low-temperature plasma simulation [29]. Reaction rates provided in Table 1 were obtained from Yuan and Raja [30] and the electron-impact cross section data used for estimating the electron transport coefficients was obtained from Turner et al. [29]. The ion mobility and diffusion coefficients were obtained from Yuan and Raja [30] and Turner et al. [29], and the diffusion coefficients for the neutral species were obtained from Turner et al. [29]. These coefficients have been listed in Table 2. Figure 1 shows the comparison of ion density obtained from MPS1D and that from Turner's PIC simulation data [29]. It should be noted that the sheath thicknesses and the peak density value at the center of the domain are very sensitive to the mobility and diffusion coefficient values for electrons and ions, and most differences can be attributed to the them. The fluid-based model (MPS1D) agrees quite reasonably with the PIC model data.

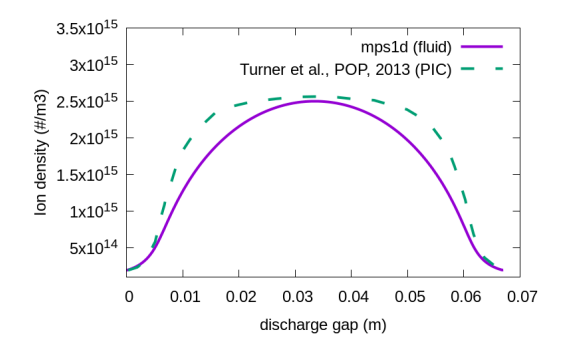


Fig. 1 Comparison of ion density obtained from MPS1D (fluid) with Turner et al.'s data (PIC) [29].

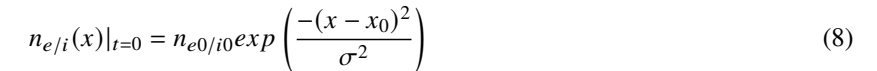
B. Solver Verification - Atmospheric Pressure Streamers

1D negative (anode-directed) streamers in nitrogen at 1 atm and 300 K were also simulated using MPS1D. The case set up was chosen to be the same as that provided in Markosyan et al. [31], where data obtained from a PIC simulation

 $\mu_k(m^2/V/s)$ $D_k(m^2/s)$ **Species** exp(54.51)-exp(55.0) $0.3942log(1.5k_bT_e)$ $1.412log(1.5k_bT_e)$ $2.134/(1.5k_bT_e)$ $0.6433/(1.5k_bT_e)^2$ $2.586/(1.5k_bT_e)$ $0.8763/(1.5k_bT_e)^2$ Ε $(0.1025)/(1.5k_bT_e)^3)/N_{gas}$ $(0.07112)/(1.5k_bT_e)^3)/N_{gas}$ $2.69 \times (1 + (1.2e - 03)(E/N)^2 + (4.2e - 08)(E/N)^4)^{(-1.0/8.0)}$ $\mu_i \times k_B T_i / e$ He⁺ $8.148 \times 10^{-5} \times (P_{atm}/P_g)$ $2.403 \times 10^{-3} \times (P_{atm}/P_g)$ He₂⁺ $4.116 \times 10^{-4} \times (P_{atm}/P_{o})$ He* $2.029 \times 10^{-4} \times (P_{atm}/P_{o})$ He₂*

Table 2 List of mobilities and diffusion coefficients used for the He CCP discharge [29, 30].

has been used to verify a higher-order moment model and a first-order drift-diffusion (DD) model for 1D streamer simulations. A Gaussian seed was initialized with an equal peak density of electrons and ions near the cathode, given by Eq. 8, where $n_{e0/i0} = 2 \times 10^{18} m^{-3}$, $\sigma = 0.029$ mm and $x_0 = 0.8$ mm. The domain length was set to 1.2 mm and 1025 uniformly spaced grid points were used for this simulation with MPS1D. The local-field approximation (LFA) was used, where the ionization rate constant, electron mobility and diffusivity were fit as functions of the local reduced electric field (E/N), based on the plots for these quantities in Dujko et al. [32]. As expected, the electrons drift towards the anode while ionizing the bulk of the neutral gas. The ions are assumed to be immobile in comparison to the electrons. This relative drift of electrons creates a thin region of space charge which then keeps propagating under the effect of the external electric field (E/N = 590 Td in this case). As this region of negative space charge propagates towards the anode, it distorts the external field due to the opposite direction of its own field. The streamer propagation (time varying electron number density) and the resultant electric field are shown in Fig. 2 (a) and (b) at three different time instances of 0.07 ns, 0.35 ns and 0.7 ns. As can be seen, MPS1D compares reasonably well with the drift-diffusion (DD) model based data and the PIC model based data provided in Markosyan et al. [31].



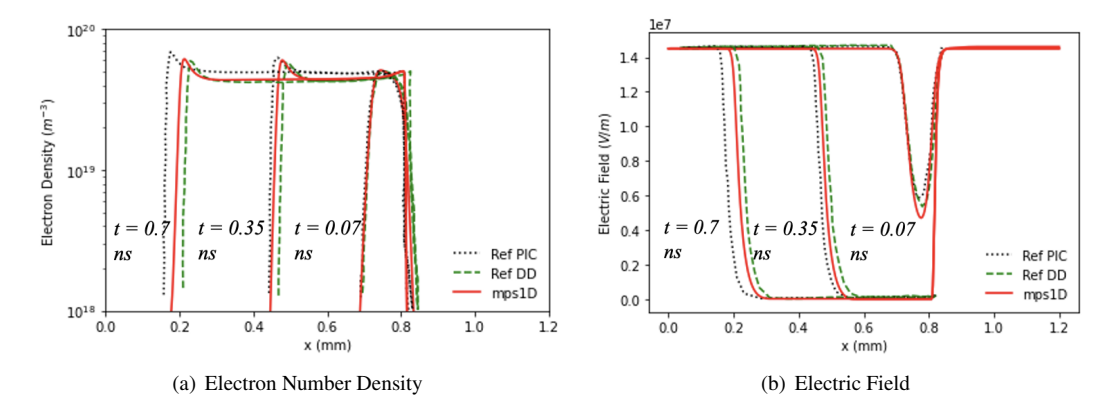


Fig. 2 Anode directed N₂ streamers: verification of MPS1D with data provided in Ref - . [31] Markosyan et al.

C. Avalanche to Streamer to Spark Transition in Air and Ammonia-Air Premixed Flame

Avalanche to streamer to spark transition has been simulated using MSP1D in air and premixed ammonia (NH₃) - air mixtures. A plasma kinetic mechanism consisting of 27 species and 78 reactions comprising of electron impact attachment, electronic excitation, dissociation, and ionization reactions of NH₃, O₂, N₂ and H₂O has been compiled as a subset of the mechanisms provided in Zhong et al. [33] and Taneja et al. [10]. The mechanism also consists of radical production reactions, which are typically formed by electron-ion recombination and quenching of electronic excited

states of these species. All simulations described in this section have been initialized with a low enough quasi-neutral background density of electrons and ions, each with a total number density of $200 \ cm^{-3}$. A gap of 4 mm discretized with 1025 uniformly spaced grid points (sufficient to achieve grid independence) has been used as the simulation domain. Moreover, a fixed time-step of 2.5×10^{-14} s, which is smaller than the smallest value of the dielectric relaxation time-scale $(\epsilon_0/\Sigma(\mu_i Z_i n_i) \approx 7.5 \times 10^{-14} s)$, has been used. The first comparison has been made in terms of the streamer formation time and location in air and in a premixed stoichiometric ammonia-air mixture at 300 K and 1 atm. The anode potential is fixed at 11.5 kV which maintains a background electric field of 28.75 kV/cm, which is slightly higher than the breakdown potential ($\sim 25 - 26kV/cm$) for air at 300 K and 1 atm. Consequently, the background reduced electric field (E/N) is set to ~ 120 Td. Three distinct phases of the plasma dynamics in air can be seen in Fig. 4 (a). The first phase is the avalanche phase, where the multiplication of electrons due to ionization and electron drift result in exponentially increasing electron densities from the cathode (x = 4 mm, right electrode) to the anode (x = 0 mm, left electrode). This follows from Townsend's theory of electron avalanche. The ions remain almost immobile when the electrons keep drifting towards the anode, which creates a space charge region.

As can be seen from Fig. 3, the natural logarithm of the electron number density varies linearly with distance, until the space charge field increases beyond the applied electric field, which forms the ionization front called the streamer. The slope of the avalanche, α , is the number of effective ionization events per unit distance. α is a function of the mean free path, which in turn depends on the thermo-chemical state and the local reduced electric field (E/N) which can strongly affect the rate of collisions. The value of α for a premixed ammonia-air mixture at 300 K and 1 atm has been determined to be ~6.73 from figure 3 (b). This value changes substantially, to ~14.02 for a discharge in pure air at the same temperature and pressure, driven by the same applied electric potential difference. This can be seen from the steeper slope of the avalanche in Fig. 4 (a). As per Meek's criterion, $\alpha d \approx 18 - 22$ at the location of streamer formation. Thus, for the ammonia air mixture, which has an $\alpha \approx 6.73$, the streamer can form anywhere between 2.67 mm and 3.25 mm away from the cathode. Figure 4 (b) shows that the streamer forms around 0.8 mm from the anode, which is 3.2 mm from the cathode. Thus, the Meek's criterion is followed. Similarly, the streamer forms at a distance of ~2.70 mm from the anode (1.3 mm from the cathode), in pure air, which falls in the range of 1.28 mm and 1.56 mm from the cathode, as prescribed by the Meek's criterion. The electric field due to the space charge opposes the applied electric field due to the higher density of drifted electrons near the anode, and a net positive charge due to higher density of the immobile ions in the bulk of the inter-electrode gap. When this value exceeds the external applied field, the electrons then start moving in the direction opposite to this net electric field, which is from the anode to the cathode, effectively driving up the ionization and electric fields at the streamer head. This can be clearly seen in Fig. 5 (a), where the electric field in the bulk decreases below the value of the applied field and keeps increasing at the streamer head, with the multiplication of electrons from the anode to the cathode, with time. Higher electric fields and increasing electron number densities also drive up the rates of progress of excitation reactions such as $e + N_2 \longrightarrow e + N_2(e)$, which in turn produces increased amounts of N₂(e) (N₂(e) are representative of three distinct electronic excited states of $N_2 - N_2(A_3)$, $N_2(B_3)$ and $N_2(C_3)$) that eventually relaxes to its ground state by liberating its energy to dissociate ground state O_2 to form O radicals and also increases the kinetic energy of the products which is manifested as fast gas heating. Similarly, the dissociative excitation of NH₃ results in the formation of H radicals, mainly by the reactions e + \rightarrow e + NH₂ + H and e + NH₃ \longrightarrow e + NH + 2 H. The most direct pathway to produce OH radicals during the discharge is through the formation of O(1D), an electronic state of O2, and its dissociative quenching to form OH via $NH_3 + O(^1D) \longrightarrow OH + NH_2$. The evolution of these radicals is shown in Fig. 5 (b).

Furthermore, there is a significant difference in the average velocity of streamer propagation in these two cases. The streamer head takes almost 25 ns to travel a distance of 3.2 mm with an average velocity of 128 km/s for the ammonia-air mixture case, whereas it only takes 3 ns to travel a distance of 1.25 mm with an average velocity of 417 km/s for the discharge in pure air. Post connection, the streamer transitions to a spark phase, where the inter-electrode gap is bridged by the plasma that results in increased amounts of current flow and intense ionization. To maintain the plasma in the non-equilibrium regime, the external voltage supply in a nanosecond pulsed plasma source is typically cut-off after a spark forms, to prevent its transition to a thermal arc plasma. The increased ionization causes an order of magnitude jump of electrons, ions, and neutral radical densities, which assist in reducing the ignition delay of fuel-air mixtures. However, further transition to an arc results in the joule heating facilitating only elastic collisions between electrons and neutrals which causes the gas temperature and electron temperature to equilibriate, thereby yielding only a gas heating effect. The reasons behind this faster streamer propagation will be investigated in our future work.

Since most non-equilibrium plasma discharge based ignition technologies work by depositing a train of repetitive nanosecond pulses, every subsequent plasma pulse is deposited in evolving thermo-chemical conditions, as the ignition kernel evolves. In the simplest case, this dependence on the local thermo-chemical state can be represented by discrete

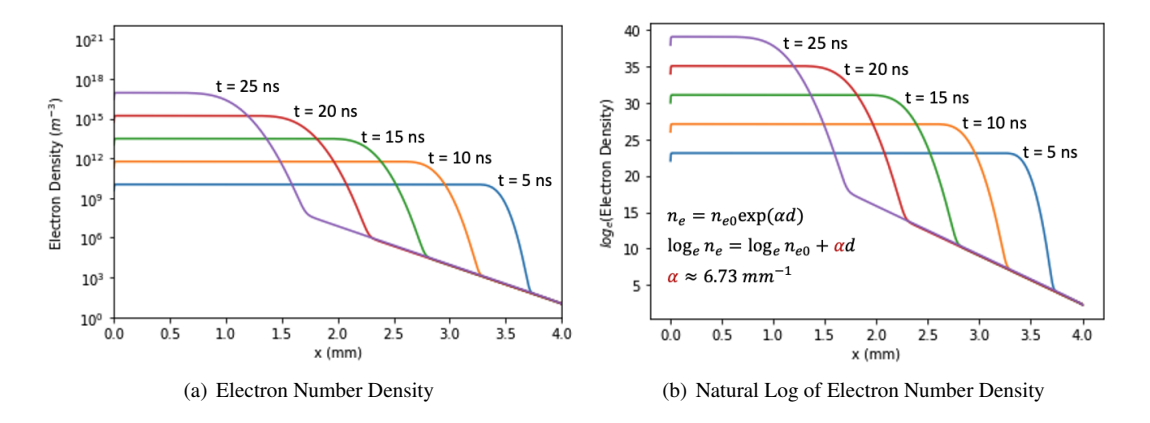


Fig. 3 Avalanche phase of the plasma in a premixed NH₃-air mixture at 300 K and 1 atm. Numbers on the curves show the sequence of electron number densities in time, which can also be seen from the legend.

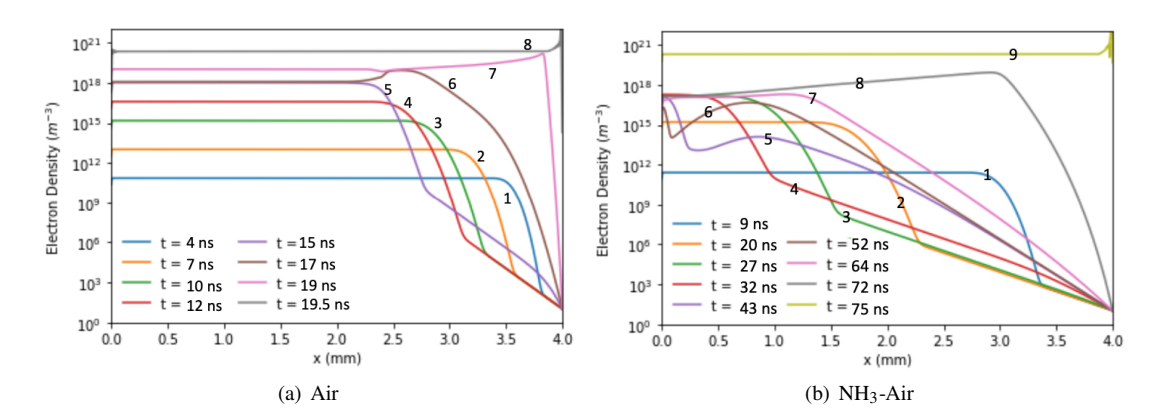


Fig. 4 Avalanche to Streamer to Spark Transition in Air and NH₃-Air mixtures. Numbers on the curves show the sequence of the quantity plotted in time, which can also be seen from the legend.

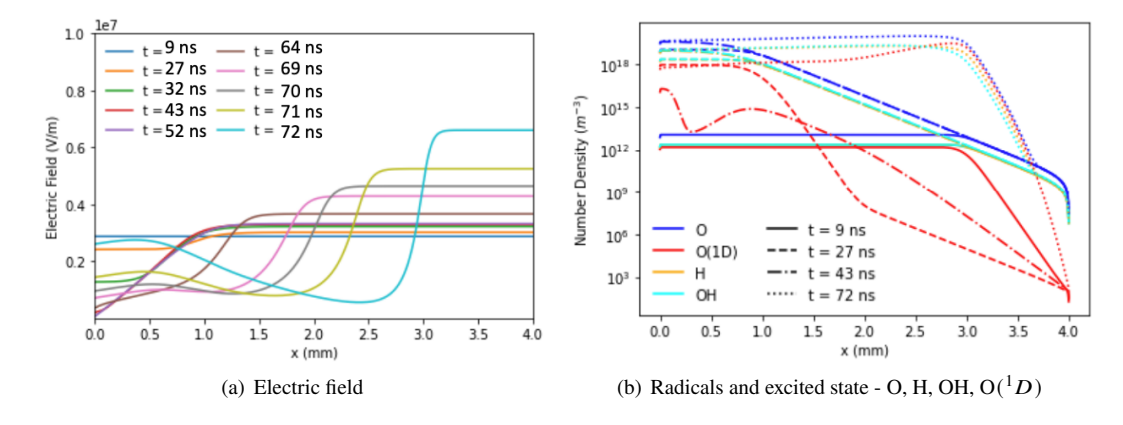


Fig. 5 Electric Field and Neutral Radical Density Evolution in $\mathrm{NH_{3} ext{-}Air}$ mixture at 300 K and 1 atm

states of a laminar premixed NH $_3$ - air flame as shown in Fig. 6 (a). The baseline case, as discussed above, was at the inlet conditions of premixed fuel and air at 300 K. The three other states shown in Fig. 6 (b), (c) and (d), represent the conditions in the pre-heat zone (1000 K, $X_{\rm NH}_3: X_{\rm O_2}: X_{\rm N_2}: X_{\rm H_2O} = 0.1288: 0.1077: 0.6330: 0.1305$), the reaction zone (1580 K, $X_{\rm NH}_3: X_{\rm O_2}: X_{\rm N_2}: X_{\rm H_2O} = 0.0554: 0.0497: 0.6662: 0.2287$) and the fully burnt zone (2035)

K, X_{NH_3} : X_{O_2} : $X_{\text{H}_2\text{O}}$ = 0.0 : 0.0 : 0.7 : 0.3). All these cases assume that the mole fractions of minor species formed are negligible, for the ease of parametrization. Figures 4 (b) and 6 (b), (c), & (d) show that the streamer formation and spark formation time vary substantially with changing thermo-chemical conditions. For these four cases, the streamer formation time varied from 45 ns (baseline, 300 K) to 6.5 ns (1000 K) to 5.0 ns (1580 K) to 4.5 ns (2035 K). Similarly, an exponential difference in the time for streamer to spark transition was observed as the temperature and mass fractions changed from the unburnt to the fully burnt state (30 ns - 300 K, 2.0 ns - 1000 K, 1.5 ns - 1580 K and 1 ns - 2035 K). These durations are certainly a strong function of the applied voltage and the inter-electrode gap distance in a 1D setting like the one used in this research, in addition to the thermochemical state. Increasing the temperature reduces the total number density (N) of the gas, which increases the reduced electric field (E/N). This increased reduced electric field (E/N) accelerates effective ionization which results in faster transition to streamer and nanosecond spark phases. To investigate if this is the only cause for the change in streamer and spark formation times, the applied reduced electric field (E/N) was then held constant (120 Td), by changing the applied voltage proportionally. However, it was observed that the three cases at the partially burnt and the fully burnt states did not breakdown and form a streamer at a background reduced electric field (E/N) of 120 Td. This is seen from Fig 7 (a). This suggests that the threshold electric field required for streamer inception varies strongly with the thermo-chemistry. Moreover, the rates of progress of different ionization and attachment reactions shown in Fig. 7 (b) also suggest that the increased concentration of N₂ and the presence of H₂O post combustion of ammonia result in faster ionization which further assists streamer formation and propagation. Future research will focus on quantifying the relative importance of these effects and how it can affect the overall distribution of electron energy which eventually determines plasma kinetics and gas heating. Getting accurate estimates of these processes are key for accurately modeling plasma assisted combustion.

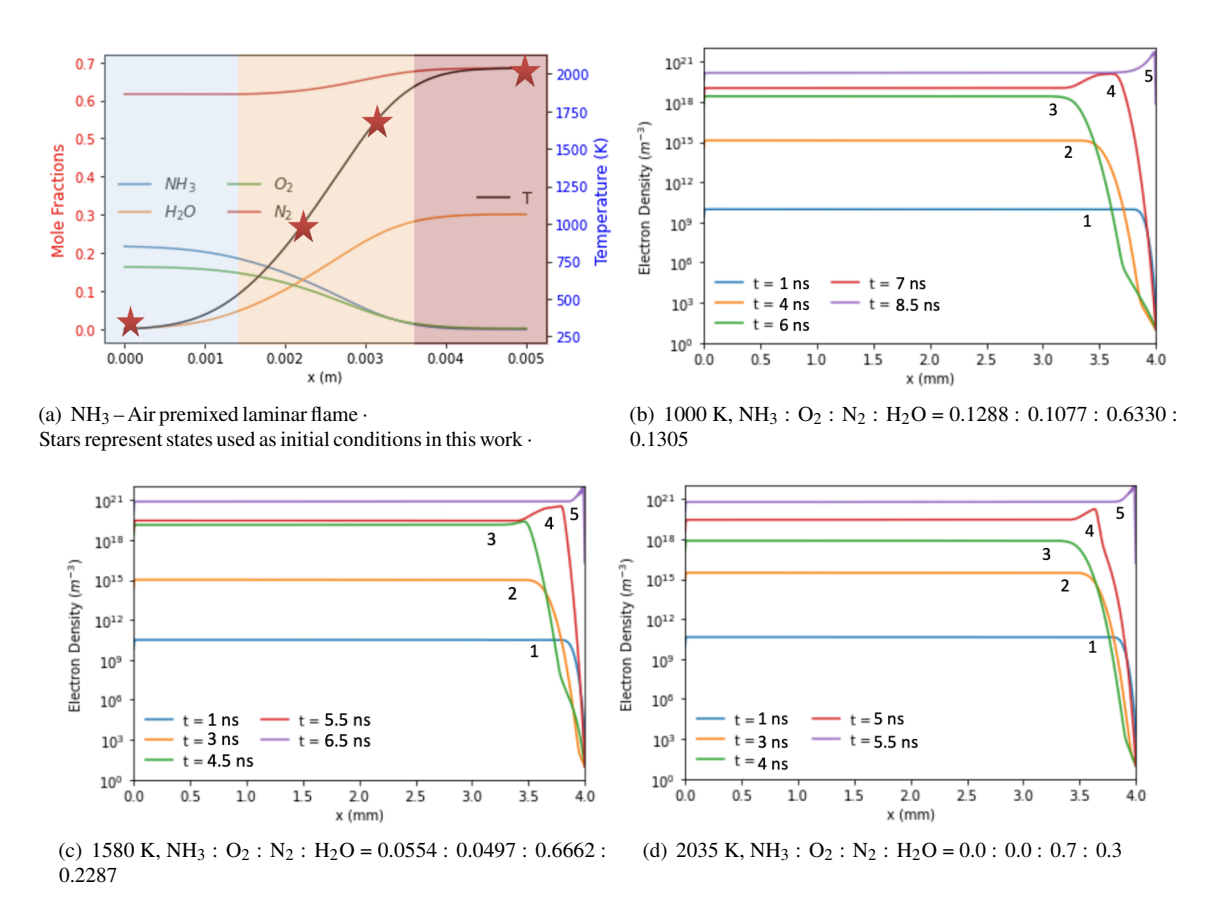
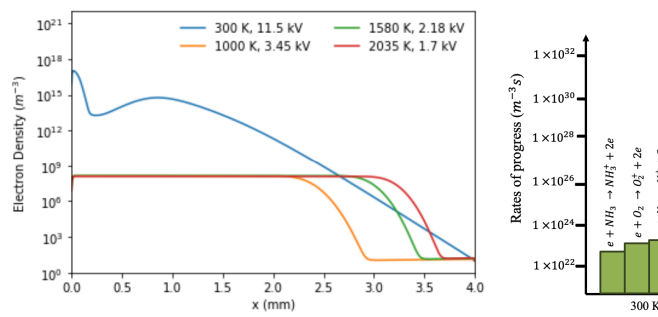
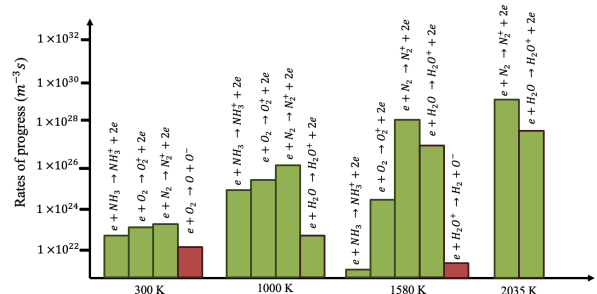


Fig. 6 Avalanche to Streamer to Spark Transition at various thermo-chemical states of an NH₃-Air flame. Numbers on the curves show the sequence of the quantity plotted in time, which can also be seen from the legend.





- (a) Electron densities for all cases at 45 ns with background E/N = 120 Td
- (b) Rates of progress of ionization (green) and attachment (red) reactions

Fig. 7 Electron Density (E/N of 11.5 kV) and Rates of Progress (constant applied voltage of 11.5 kV).

V. Conclusion

This research focused on 1D modeling of avalanche to streamer to spark transition in air and ammonia-air mixtures. The streamer formation was observed to obey the Meek's criterion for all the cases, and it was shown that the value of the number of ionization events per unit length, α , changed with the thermo-chemical state. For an applied voltage of 11.5 kV and a temperature and pressure of 300 K and 1 atm, respectively, the value of α changed from 14.02 to 6.73 for a nanosecond discharge in pure air vs. that in a premixed ammonia-air mixture. This resulted in a change in the location of streamer inception. Furthermore, a change in the average streamer propagation velocity was also observed based on the thermo-chemical state. To further assess the impact of the thermo-chemical state on the discharge kinetics and dynamics, different gas temperatures and compositions based on a laminar premixed ammonia - air flame were chosen to analyze streamer and spark formation. The streamer and spark formation time reduced almost exponentially with increasing temperature and changing the gas composition from the unburnt to the fully burnt state. While the increase in the background reduced electric field seems like an obvious reason for faster streamer and spark formation, other effects such as change of the background gas composition also seem to play a role. Moreover, dominant pathways to generate important radicals for combustion such as O, H and OH during the plasma discharge were also presented. Future research will focus on quantifying the electron energy distribution during the discharge and delineating the importance of other radical generation pathways both during and after the plasma discharge.

Acknowledgments

S. Yang acknowledges the grant support from NSF CBET 2002635. T.S. Taneja acknowledges the grant support from the NSF INTERN Supplemental Funding Opportunity and the University of Minnesota (UMN) Doctoral Dissertation Fellowship (DDF). This work was authored in part by the National Renewable Energy Laboratory, operated by Alliance for Sustainable Energy, LLC, for the U.S. Department of Energy (DOE) under Contract No. DE-AC36-08GO28308. Funding provided by U.S. Department of Energy's Laboratory Directed Research and Development (LDRD) is acknowledged. The views expressed in the article do not necessarily represent the views of the DOE or the U.S. Government. The U.S. Government retains and the publisher, by accepting the article for publication, acknowledges that the U.S. Government retains a nonexclusive, paid-up, irrevocable, worldwide license to publish or reproduce the published form of this work, or allow others to do so, for U.S. Government purposes.

References

- [1] Raizer, Y. P., and Allen, J. E., Gas discharge physics, Vol. 1, Springer, 1991.
- [2] Townsend, J. S., "XVII. The Conductivity produced in gases by the motion of negatively charged ions," *The London, Edinburgh, and Dublin Philosophical Magazine and Journal of Science*, Vol. 1, No. 2, 1901, pp. 198–227.
- [3] Loeb, L. B., and Meek, J. M., "The mechanism of spark discharge in air at atmospheric pressure. I," *Journal of applied physics*, Vol. 11, No. 6, 1940, pp. 438–447.
- [4] Meek, J., "A theory of spark discharge," Physical review, Vol. 57, No. 8, 1940, p. 722.

- [5] Naidis, G., "Simulation of streamer-to-spark transition in short non-uniform air gaps," *Journal of physics D: Applied physics*, Vol. 32, No. 20, 1999, p. 2649.
- [6] Bouwman, D., Teunissen, J., and Ebert, U., "3D particle simulations of positive air–methane streamers for combustion," *Plasma Sources Science and Technology*, Vol. 31, No. 4, 2022, p. 045023.
- [7] Nijdam, S., Teunissen, J., and Ebert, U., "The physics of streamer discharge phenomena," *Plasma Sources Science and Technology*, Vol. 29, No. 10, 2020, p. 103001.
- [8] Naidis, G., "Modelling of transient plasma discharges in atmospheric-pressure methane–air mixtures," *Journal of Physics D: Applied Physics*, Vol. 40, No. 15, 2007, p. 4525.
- [9] Choe, J., Sun, W., Ombrello, T., and Carter, C., "Plasma assisted ammonia combustion: Simultaneous NO_x reduction and flame enhancement," *Combust. Flame*, Vol. 228, 2021, pp. 430–432.
- [10] Taneja, T. S., Johnson, P. N., and Yang, S., "Nanosecond pulsed plasma assisted combustion of ammonia-air mixtures: Effects on ignition delays and NOx emission," *Combustion and Flame*, Vol. 245, 2022, p. 112327.
- [11] Faingold, G., Kalitzky, O., and Lefkowitz, J. K., "Plasma reforming for enhanced ammonia-air ignition: a numerical study," Fuel Communications, Vol. 12, 2022, p. 100070.
- [12] Shahsavari, M., Konnov, A. A., Valera-Medina, A., and Jangi, M., "On nanosecond plasma-assisted ammonia combustion: Effects of pulse and mixture properties," *Combustion and Flame*, Vol. 245, 2022, p. 112368.
- [13] Mao, X., Zhong, H., Liu, N., and Ju, Y., "Ignition enhancement of NH3/air mixtures by non-equilibrium excitation in a nanosecond pulsed plasma discharge," AIAA SCITECH 2023 Forum, 2023, p. 0748.
- [14] Tang, Y., Xie, D., Wei, C., Huang, B., Shi, B., and Wang, N., "Effect of microsecond repetitively pulsed discharges on lean blow-off limit and emission of rapidly-mixed ammonia/air swirling flames," *Applications in Energy and Combustion Science*, 2023, p. 100140.
- [15] Taneja, T. S., and Yang, S., "Numerical modeling of plasma assisted pyrolysis and combustion of ammonia," AIAA Scitech 2021 Forum, 2021, p. 1972.
- [16] Johnson, P. N., Taneja, T. S., and Yang, S., "Plasma-based global pathway analysis to understand the chemical kinetics of plasma-assisted combustion and fuel reforming," *Combustion and Flame*, Vol. 255, 2023, p. 112927.
- [17] Johnson, P. N., Taneja, T. S., and Yang, S., "Global pathway analysis of plasma assisted ammonia combustion," AIAA Scitech 2022 Forum, 2022, p. 0977.
- [18] Guerra-Garcia, C., and Pavan, C. A., "The backward problem in plasma-assisted combustion: Experiments of nanosecond pulsed discharges driven by flames," *Applications in Energy and Combustion Science*, 2023, p. 100155.
- [19] Sitaraman, H., and Grout, R., "Premixed combustion simulations with a self-consistent plasma model for initiation," 54th AIAA Aerospace Sciences Meeting, 2016, p. 2158.
- [20] Yang, S., Nagaraja, S., Sun, W., and Yang, V., "Multiscale modeling and general theory of non-equilibrium plasma-assisted ignition and combustion," *Journal of Physics D: Applied Physics*, Vol. 50, No. 43, 2017, p. 433001.
- [21] Yang, S., Gao, X., Yang, V., Sun, W., Nagaraja, S., Lefkowitz, J. K., and Ju, Y., "Nanosecond pulsed plasma activated C2H4/O2/Ar mixtures in a flow reactor," *Journal of Propulsion and Power*, Vol. 32, No. 5, 2016, pp. 1240–1252.
- [22] Rousso, A., Yang, S., Lefkowitz, J., Sun, W., and Ju, Y., "Low temperature oxidation and pyrolysis of n-heptane in nanosecond-pulsed plasma discharges," *Proceedings of the Combustion Institute*, Vol. 36, No. 3, 2017, pp. 4105–4112.
- [23] Chen, T. Y., Taneja, T. S., Rousso, A. C., Yang, S., Kolemen, E., and Ju, Y., "Time-resolved in situ measurements and predictions of plasma-assisted methane reforming in a nanosecond-pulsed discharge," *Proceedings of the Combustion Institute*, Vol. 38, No. 4, 2021, pp. 6533–6540.
- [24] Sitaraman, H., and Raja, L., "Gas temperature effects in micrometre-scale dielectric barrier discharges," *Journal of Physics D: Applied Physics*, Vol. 44, No. 26, 2011, p. 265201.
- [25] Hayashi, M., "Personal communication to the JILA atomic collisions data center,", 1987.

- [26] Hagelaar, G., "Brief documentation of BOLSIG+ version 03/2016," *Laboratoire Plasma et Conversion dEnergie (LAPLACE)*, *Universit Paul Sabatier*, Vol. 118, 2016.
- [27] Pancheshnyi, S., Eismann, B., Hagelaar, G., and Pitchford, L., "Computer code ZDPlasKin, University of Toulouse, Laplace," Tech. rep., CNRS-UPS-INP, Toulouse, France www. zdplaskin. laplace. univ-tlse. fr, 2008.
- [28] Reusken, A., "Convergence of the multilevel full approximation scheme including the V-cycle," *Numerische Mathematik*, Vol. 53, 1988, pp. 663–686.
- [29] Turner, M. M., Derzsi, A., Donko, Z., Eremin, D., Kelly, S. J., Lafleur, T., and Mussenbrock, T., "Simulation benchmarks for low-pressure plasmas: Capacitive discharges," *Physics of Plasmas*, Vol. 20, No. 1, 2013, p. 013507.
- [30] Yuan, X., and Raja, L. L., "Computational study of capacitively coupled high-pressure glow discharges in helium," *IEEE Transactions on Plasma Science*, Vol. 31, No. 4, 2003, pp. 495–503.
- [31] Markosyan, A., Dujko, S., and Ebert, U., "High-order fluid model for streamer discharges: II. Numerical solution and investigation of planar fronts," *Journal of Physics D: Applied Physics*, Vol. 46, No. 47, 2013, p. 475203.
- [32] Dujko, S., Markosyan, A., White, R., and Ebert, U., "High-order fluid model for streamer discharges: I. Derivation of model and transport data," *Journal of Physics D: applied physics*, Vol. 46, No. 47, 2013, p. 475202.
- [33] Zhong, H., Mao, X., Liu, N., Wang, Z., Ombrello, T., and Ju, Y., "Understanding non-equilibrium N2O/NOx chemistry in plasma-assisted low-temperature NH3 oxidation," *Combustion and Flame*, Vol. 256, 2023, p. 112948.